Research Paper

The Holocene
1–14

DOI: 10.1177/09596836251378034
journals.sagepub.com/home/hol
Sage

Multi-regional calibration of *Patella caerulea* as a palaeothermometer using oxygen isotope values and Mg/Ca ratios

Danai Theodoraki,[1,2] Marcello A Mannino,[3] Amy L Prendergast,[4] Bernd R Schöne[5] and Niklas Hausmann[1]

Abstract

This study presents a comprehensive calibration of the *Patella caerulea* as a palaeotemperature archive across the Central and Eastern Mediterranean, focusing on Mg/Ca ratios and $\delta^{18}O$ values. We analysed 131 modern specimens collected from 22 localities, with a focus on the Aegean region. Our results demonstrate strong correlations between Mg/Ca ratios and the temperature proxy $\delta^{18}O_{shell}$, with a mean R^2 value of 0.89. These findings reinforce the utility of Mg/Ca as a reliable, though specimen-specific, proxy for relative SST variations, supporting its role in reconstructing seasonal temperature patterns and revealing areas of interest for subsequent methods. Additionally, oxygen isotope data from both shells and water samples at selected sites agreed well with element chemical data (Mg/Ca), confirming the usefulness of SST estimates based on $\delta^{18}O$ values as well as the season of death in ~80% of studied specimens. Findings of the present study enhance our understanding of the applicability of *P. caerulea* as a palaeotemperature archive and provide a robust baseline for future palaeoclimate studies in Mediterranean archaeological contexts.

Keywords

Laser-induced breakdown spectroscopy, Mediterranean, Mg/Ca ratios, *Patella* sp., sclerochronology, stable oxygen isotopes

Received 15 April 2025; revised manuscript accepted 8 August 2025

Introduction

Shells of the *Patella* genus have been shown to serve as reliable palaeothermometers using oxygen isotope analysis (Colonese et al., 2012; Fenger et al., 2007; Ferguson et al., 2011; Gutiérrez-Zugasti et al., 2017; Prendergast and Schöne, 2017; Shackleton, 1973) and more recently Mg/Ca ratios (Cobo et al., 2017; Hausmann et al., 2019a, 2023). The study of *Patella* spp. and other limpet shells as palaeothermometers or indicators for season of capture in archaeological sites has a long history (Colonese et al., 2011, 2012; Deith and Shackleton, 1988; Fenger et al., 2007; García-Escárzaga et al., 2020; Parker et al., 2020; Shackleton, 1973; Surge and Barrett, 2012; Wang et al., 2012). Among gastropods, limpet shells are the most commonly studied molluscs due to their simple anatomy and ubiquity along most of the world's rocky shorelines (Hausmann, 2024).

Limpets were collected by past human societies not only for consumption but also as tools, bait or adornments, among others. The study of shells from archaeological contexts can contribute to the reconstruction of human diet, environmental conditions, manufacture and use of artefacts, marine resources exploitation and management and seasonality of activities (Bar-Yosef Mayer, 2005; Çakirlar, 2014; Claassen, 1998; Firth, 2021). The relatively short life-span of limpets makes the shells advantageous for the study of short-term climatic events, and their sessility for the study of site-specific climatic events. Additionally, since they are commonly found in archaeological contexts their direct connection enables us to relate palaeoenvironmental and palaeoclimatic data to the broader archaeological context of the site, linking environmental change with past human activities (Leng and Lewis, 2016; West et al., 2018).

Before applying geochemical analyses to archaeological samples, it is essential to first validate the technique using modern samples from the same species and similar locations. This has been done on *Patella* spp. shells before in various parts of the world, including South Africa, Spain, Argentina, Scotland, the Gibraltar strait (North Africa and South Europe) and parts of the Mediterranean (Colonese et al., 2012; Fenger et al., 2007; Ferguson et al., 2011; Gutiérrez-Zugasti et al., 2017, 2025; Prendergast and Schöne, 2017; Shackleton, 1973). Researchers in these studies detected regional offsets in shell $\delta^{18}O$ values from equilibrium with surrounding water. This offset was attributed to so-called 'physiological' (Epstein et al., 1951) or 'vital' effects (Urey et al., 1951) that may disrupt isotopic equilibrium of the shells and is typically species-specific. These effects refer to metabolic processes that influence how environmental information is captured in the geochemical composition of biogenic hard structures (Schöne et al., 2011). The offset can be incorporated into

[1]Leibniz-Zentrum für Archäologie, Germany
[2]Vor- und Frühgeschichtliche Archäologie, University of Mainz, Germany
[3]Department of Archeology and Heritage Studies, Aarhus University, Denmark
[4]School of Geography, University of Melbourne, Australia
[5]Institute of Geosciences, University of Mainz, Germany

Corresponding author:
Danai Theodoraki, Leibniz-Zentrum für Archäologie, Mainz, Germany & Vor- und Frühgeschichtliche Archäologie, University of Mainz, Ludwig-Lindenschmit-Forum 1, Mainz 55116, Germany.
Email: danai.theodoraki@leiza.de

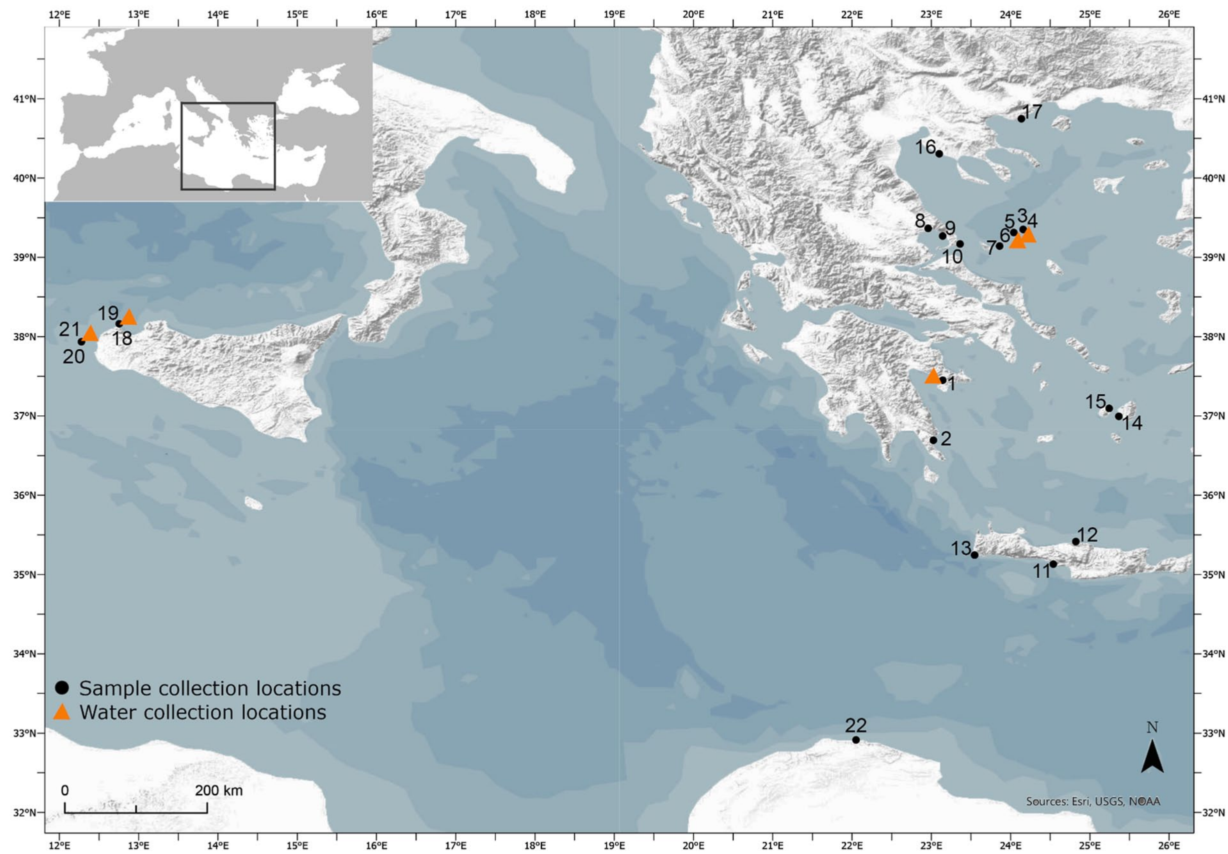

Figure 1. Geographical distribution of modern shell collection locations. Numbers correspond to Table 1. Orange triangles indicate the location of the water samples. Locations: 1. Franchthi, 2. Monemvasia, 3. Youra island (west coast), 4. Youra island (south coast), 5. Agios Petros island, 6. Kyra-Panagia island, 7. Patitiri, Alonnisos island, 8. Plakes, Volos, 9. Koropi, Pagasetic Gulf, 10. Katiyorgis, Aegean sea, 11. Ligres, Rethymno, 12. Glaros, Rethymno, 13. Kedrodasos, Chania, 14. Alyko, Naxos island, 15. Ysterni, Paros island, 16. Nea Kallikrateia, Chalkidiki, 17. Pyrgos Apollonias, Kavala, 18. Tonnara del Secco (east), 19. Tonnara del Secco (west), 20. Faro Punta Sottile (east), 21. Faro Punta Sottile (west), 22. Sousa.

palaeotemperature equations as a correction factor to adjust SST estimates from archaeological shells, for example, where the direct measurement of $\delta^{18}O_{water}$ is not possible. However, the geographic extent within which this offset can be applied have not yet consistently been looked at across multiple localities. Given the use of limpet shells as palaeothermometers in climate studies (Surge and Barrett, 2012; Wang et al., 2012), getting a better understanding of any offset is useful for future reconstruction of palaeoclimate.

Previous work on limpet specimens from the Eastern Mediterranean has demonstrated the efficacy of using *P. caerulea* shells as high-resolution archives of SST (Prendergast and Schöne, 2017). Results of an in-depth oxygen isotope and sclerochronological analysis of 19 modern shells from eight Mediterranean sites (Tunisia, Malta, Libya, Croatia, Turkey, Israel) provided evidence on the reliability of *P. caerulea* shells as palaeothermometers. These same shells have subsequently been studied for Mg/Ca ratios to explore the use of this proxy (Hausmann et al., 2019a), with results being generally reliable but specimen-specific variability of Mg/Ca even among coeval animals pointed towards additional influences impacting on the element chemical (Mg/Ca) record.

Here, we aim to expand on this initial dataset by studying a wider range of localities (Figure 1) and an increased number of specimens, with a particular focus on the Mg/Ca composition of the shells. In addition, in the case where there were archaeological sites in the vicinity, we also studied the oxygen isotope composition of shells and the oxygen isotope signature of (modern) local water to best support future palaeoclimate studies.

Materials and methods

Materials

Our dataset consists of 131 *P. caerulea* specimens from 22 localities within the Central and Eastern Mediterranean (Table 1). The majority of these are located in the Aegean (17), with further sites in Italy (4) and Libya (1) (Figure 1). This spatial distribution is also reflected in the number of specimens collected (Greece: 102; Italy: 17; Libya: 12). Specimens were collected on a single occasion at each locality and at different seasons of the year, with most shells collected during autumn (61), followed by spring (44) and summer (14), while only 5 were gathered during winter.

Shells from Greece come from two collection sites located in the Peloponnese (one in proximity to the archaeological site of Franchthi; (Jacobsen et al., 1988), eight in Thessaly (four in proximity to the archaeological sites of Cyclops Cave and Agios Petros), three on Crete, two in the Cyclades and two in Northern Greece. Limpet shells from Sicily were collected in the Trapani province (near the archaeological site of Grotta dell'Uzzo) and the island of Favignana (near the archaeological site of Grotta d'Oriente). Modern shells from Sousa in Libya had been collected and analysed in the past in relation with palaeoclimatic work at the archaeological site of Haua Fteah (Prendergast and Schöne, 2017).

In the Aegean, SST is controlled by latitude and season (Poulos et al., 1997; Uçkaç, 2005). At the study localities, the SST maximum occurred in August (27℃) and the minimum in February (14℃) (Good et al., 2020; Poulos et al., 1997; Uçkaç, 2005). Generally, SST in the Aegean has rapidly increased since the 1990s, especially in the southern part of the basin (Skliris et al., 2011). The monthly mean SST from Franchthi, the island of

Table 1. Site provenance and collection dates of modern reference shells.

No.	Country	Geographic region	Collection site	Archaeological site	Site code	Coordinates	Collection date	No. of limpets analysed
1	Greece	Peloponnese	Franchthi	Franchthi	FR-P	37.42280, 23.13084	15/05/2021	24
2	Greece	Peloponnese	Monemvasia		ML	36.68648, 23.03960	17/12/2021	5
3	Greece	Thessaly	Youra isl. (west)	Cyclop's cave	Y-W	39.37678, 24.14985	17/09/2021	12
4	Greece	Thessaly	Youra isl. (south)	Cyclop's cave	Y-S	39.36861, 24.14602	17/09/2021	8
5	Greece	Thessaly	Agios Petros isl.	Agios Petros	KP-AP	39.32127, 24.05445	17/09/2021	15
6	Greece	Thessaly	Kyra-Panagia isl.		KP-KO	39.31602, 24.06613	17/09/2021	4
7	Greece	Thessaly	Patitiri, Alonnisos isl.		PA	39.14285, 23.86363	18/09/2021	5
8	Greece	Thessaly	Plakes, Volos		V-P	39.34755, 22.97251	16/09/2021	3
9	Greece	Thessaly	Koropi, Pagasetic Gulf		KO-PG	39.28927, 23.14363	10/09/2021	5
10	Greece	Thessaly	Katiyorgis, Aegean sea		V-KB	39.17255, 23.34283	17/09/2021	6
11	Greece	Crete	Ligres, Rethymno		RE-L	35.13481, 24.53191	06/08/2021	2
12	Greece	Crete	Glaros, Rethymno		RE-G	35.41310, 24.82722	05/08/2021	1
13	Greece	Crete	Kedrodasos, Chania		K-CH	35.26844, 23.55886	27/07/2021	1
14	Greece	Cyclades	Alyko, Naxos isl.		AN	36.98486, 25.38561	06/08/2021	3
15	Greece	Cyclades	Ysterni, Paros isl.		GYP	37.08777, 25.26442	14/08/2021	2
16	Greece	Macedonia	Nea Kallikrateia, Chalkidiki		NKC-M	40.30134, 23.08626	20/06/2021	4
17	Greece	Macedonia	Pyrgos Apollonias, Kavala		PARK	40.74020, 24.14294	01/09/2021	2
18	Italy	Sicily	Tonnara del Secco (east)	Grotta dell'Uzzo	TS-E	38.16794, 12.77000	16/05/2023	5
19	Italy	Sicily	Tonnara del Secco (west)	Grotta dell'Uzzo	TS-W	38.16694, 12.76886	16/05/2023	3
20	Italy	Favignana isl.	Faro Punta Sottile (east)	Grotta d'Oriente	FPS-E	37.93606, 12.27472	18/05/2023	4
21	Italy	Favignana isl.	Faro Punta Sottile (west)	Grotta d'Oriente	FPS-W	37.93521, 12.27333	18/05/2023	5
22	Libya	Cyrenaica	Sousa	Haua Fteah	MP6, M0, MBRP	32.90801, 22.04439	Spring, Summer, Autumn	12
	Total							131

Youra, Tonnara del Secco and Faro Punta Sottile are depicted in Figure 2. Slightly different seasonal SSTs have been recorded at the different localities with annual minima around 15°C and maxima around 27°C. Southern Greek sites are generally warmer. Lowest summer and winter temperatures were recorded on the island of Youra. Sea surface salinity (SSS) in the Central Mediterranean is around 38 (European Union-Copernicus Marine Service, 2016), while at the location of Cala Grande, on the south eastern side of Faro Punta Sottile, the mean psu values measured in 2002–2004 were 35.89 ± 0.088 (Mannino et al., 2008). The Aegean is additionally influenced seasonally by low-salinity water inflow from the Black Sea most time of the year. This particularly affects the sites on Youra from June to November when salinity can decline to values as low as 31 psu (Aydogdu et al., 2023; Ozer et al., 2022; Uçkaç, 2005).

Methods

The geochemical study involved the use of laser induced breakdown spectroscopy (LIBS) for Mg/Ca analysis and isotope ratio mass spectrometry (IRMS) to obtain oxygen isotope values ($\delta^{18}O$). Prior to the analysis, *Patella* spp. shells were physically cleaned with tap water to remove any adhering organic tissue before being dried overnight at room temperature. To quantify morphometric differences, the length and width of the shells was measured (Supplemental Figure S.1 and Table S.1, available online). Shells were then sectioned with a slow-speed saw (Buehler Isomet 1000) equipped with a wafering thin diamond-coated blade (0.4 mm) along the maximum growth axis. One half was retained, while the other one was used for both LIBS and oxygen isotope analysis.

Laser induced breakdown spectroscopy (LIBS)

LIBS is an analytical technique used to determine the elemental composition of materials, in this case the chemical characterisation of different shell portions. LIBS is a rapid, micro-destructive analytical technique that provides element chemical results in near-real-time, while minimal or no sample preparation is required (Cremers and Radziemski, 2006, 2013). In this study, a customised micro-LIBS instrument was used at the Leibniz Centre for Archaeology in Mainz, Germany, designed for generating Mg/Ca maps of marine shells (see Hausmann et al., 2023) for a detailed description of the analytical protocols). In short, we targeted a pulsed laser (1064 nm, 1–2 mJ, 100 Hz) on a 20–30 µm area on the sample surface, which generated a plasma plume. Emitted light from the plume was recorded by a spectrometer (0.5 µs delay, 10 µs integration time), capturing the emission lines for magnesium (MgII: 279.553 nm) and calcium (CaII: 315.887 nm). Based on the signal intensities a ratio between Mg and Ca was computed (Mg/Ca), which has a linear relationship with the molar concentration. Mg/Ca are thus reported in arbitrary units of the two emission lines as 'intensity ratios', not molar ratios. This intensity ratio and the molar ratio are however strongly correlated (Hausmann et al., 2017). Based on this correlation and to give an example, we interpret our range in Mg/Ca intensity ratio from 0.5 (winter) to 0.9 (summer) as being roughly equivalent to molar ratios of 10 and 40 mmol/mol. This correlation is, however, dependent on the chosen emission lines and spectral resolution (Cobo et al., 2017). More accurate molar ratios using LIBS can be acquired using multiple emission lines in a calibration-free system (Martínez-Minchero et al., 2023). Studies on other limpet shells have also shown that specimen specific offsets occur frequently and that relative changes in Mg/Ca rather than specific absolute ratios in mmol/mol are key for the interpretation of seasonal SST changes (Hausmann et al., 2019a, 2024).

First, a scan of the entire shell section was carried out at a 100 µm resolution and higher resolution maps at 30 µm were made for the more recent growth records along the shell aperture. Second, line scans at 30 µm resolution were run from the aperture (last growth shell portion prior to death) towards the shell apex to provide a dataset that can be directly compared to sequential oxygen isotope data. For the determination of the season of capture both maps and line scans were taken into account. In both we

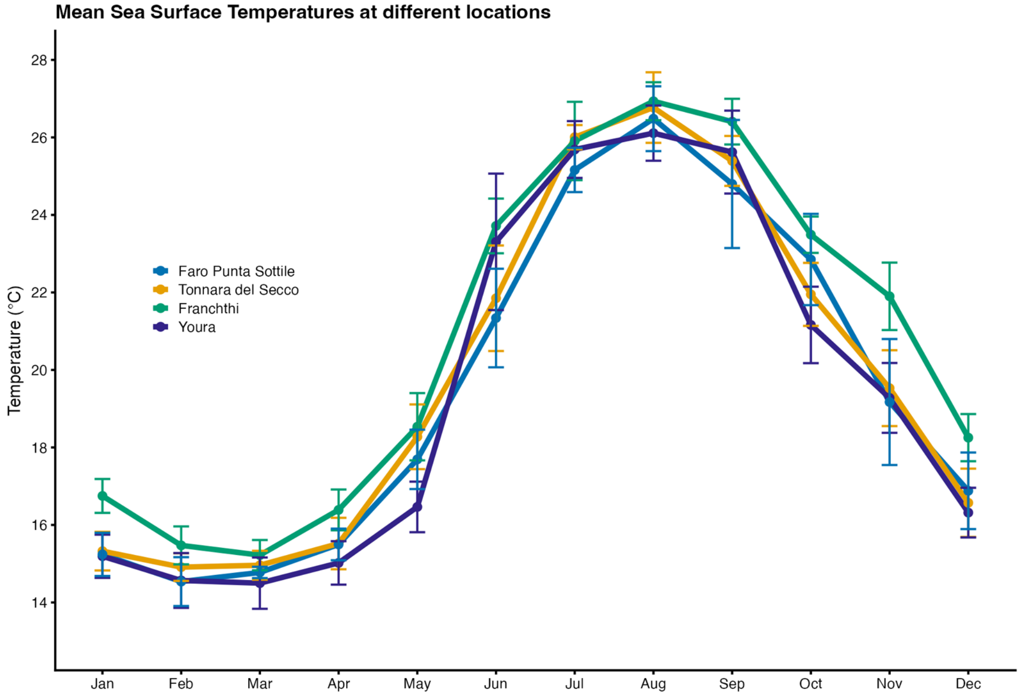

Figure 2. Monthly Sea surface temperature (SST). Instrumental data from 2011 to 2021 from Franchthi, Youra isl., Tonnara del Secco and Favignana isl. (Good et al., 2020). Error bars represent standard deviation values.

examined relative increases and decreases in Mg/Ca. These variations can be more evident in line scans, whereas in maps their consistency across a growth increment can be assessed.

Based on previous studies, limpet shell Mg/Ca is positively correlated to water temperature (Cobo et al., 2017; Ferguson et al., 2011; García-Escárzaga et al., 2018; Hausmann et al., 2019a, 2024; King et al., 2025). To interpret the Mg/Ca results, we attributed shell growth bands of lower and higher Mg/Ca ratios to certain seasons (i.e. winter or summer, respectively). In winter growth bands, Mg/Ca ratios typically fluctuated between 0.5 and 0.6, while in shell portions produced during summer, Mg/Ca ratios ranged between 0.75 and 0.90. Autumn and spring increments are identified in the intermediate values. The line scans performed on the samples were also used alongside the maps to understand seasonal cyclicity patterns, by visually identifying lower and higher Mg/Ca ratios and thus identify the seasons recorded in the shell. Note that each shell's Mg/Ca record has an individual response to SST changes and thus only relative SST changes can reliably be detected, not absolute SST values (Hausmann et al., 2024). Determining the season of capture in Mg/Ca records of limpets relies more on visual assessments than in other geochemical proxies. For instance, $\delta^{18}O$-sequences can use statistical means of separating the year into different seasons, by using upper and lower quartiles for winter and summer, and the interquartile range for spring or autumn depending on the direction of the sequence (upward or downward). In Mg/Ca records this approach is not as straightforward, since one growth increment, representing one time slice, can have a range of Mg/Ca ratios (Hausmann et al., 2019a, 2019b). The cyclical trend indicating seasonal SST changes, becomes most visible when the entirety of the growth increment is assessed instead of only a line scan, which is restricted to a specific part of the increment. While these line scans do show cyclical trends, their annual minima and maxima, which determine the values of quartiles, are not always comparable between years as the growth of the limpet shell is not always uniform. We thus rely on visual assessment of the 2D map, where we first assess the predictability of the cyclical change based on the distinctiveness of high Mg/Ca (summer) and low Mg/Ca (winter) parts of the maps, as well as the smoothness of the change between seasons, indicating that there are not major growth stops. Then, we compare the terminal growth increments to the rest of the shell record and decide which part of the cyclical change (i.e. which season) it compares best to. This is then the season of death we allocate to the specimen (see also Supplemental Figure S2, available online).

Oxygen isotope analyses

Oxygen isotope analysis is commonly applied to extract the palaeotemperature data from calcium carbonate or other materials (Craig, 1957; Epstein et al., 1953; Urey, 1947). Here, we obtained a total of 374 calcium carbonate samples from 20 shells (on average, 16, minimum = 1, maximum = 38 samples per specimen) for oxygen isotope analysis (Table 3 and Supplemental Material III, available online). Apertural and sequential carbonate samples were extracted. From these twenty specimens, fourteen were used for sequential sampling, while six provided apertural samples only (FR-P_20210515_A, B, D, E, F, J). Samples included specimens from Franchthi Paralia, south and west Youra, east and west Faro Punta Sottile and east and west Tonnara del Secco, in order to compare $\delta^{18}O$ as a proxy for palaeotemperature with the employed LIBS methodology.

To prepare the selected samples for oxygen isotope analysis, shell halves were mounted on plexiglass cubes using a plastic epoxy (Multipower 3, GlueTec). Then, to prevent fracturing under the saw's pressure, the shells were covered with a metal epoxy resin (WIKO 05), before cutting the shells into three-millimetre thick sections along their maximum growth axis with a low-speed precision saw (Buehler, Isomet 1000). Once prepared, the sections were ground on glass plates with 800 and 1200 grit powder, then polished using a 1 µm aluminium oxide (Al_2O_3) suspension on a BuehlerMasterTex cloth. After each grinding and polishing step, the sections were rinsed with water, placed in an ultrasonic bath to remove any powder grains and then air-dried (Hallmann et al., 2009). After preparing the thick sections, micromilling was done using a binocular stereoscope. The drill was mounted directly onto the microscope, while the sample was held by hand. The sampling of the carbonate powder samples was conducted parallel to the growth increments and perpendicular to the direction of growth allowing for high-resolution sampling using the Mg/Ca ratio maps as well as the high-resolution macro photographs of cross-sections of shells as a guide. Oxygen isotope analysis of shell carbonate was performed with a Thermo Fisher Scientific MAT 253 continuous flow – IRMS equipped with a GasBench II, located at the Geosciences Institute of the Johannes Gutenberg University of Mainz. Samples were calibrated against an in-house Carrara marble with an $\delta^{18}O$ value of +2.01‰. Results are given relative to V-PDB. The average 1σ precision computed from eight injections per sample was better than 0.08‰, and long-term accuracy of the machine (=421 blindly measured NBS-19 samples) was better than 0.04‰.

Furthermore, isotope analyses were run on water samples from 6 locations (Franchthi, Youra island (south coast), Agios Petros island, east and west Tonnara del Secco and from west Faro Punta Sottile). Measurements were performed with a Picarro (L2140-i) spectrometer at the Max Planck Institute for Chemistry in Mainz, following the method described by de Graaf et al. (2021). The data produced was post-processed for scale conversion to VSMOW using a 2-point calibration based on two in-house standards (MainzTap, 2022, with a $\delta^{18}O$ value of −8.75‰ VSMOW and a $\delta^{2}H$ value of −63.53‰ VSMOW, and Kona 2022, $\delta^{18}O$ = 1.52‰ VSMOW and a $\delta^{2}H$ = 3.48‰ VSMOW). We used the locality-specific $\delta^{18}O_{water}$ values and the palaeotemperature equation by (Hays and Grossman, 1991) to reconstruct SST values.

$$T_{\delta^{18}O}\left(°C\right) = 15.7 - 4.36 * \left(\delta^{18}O_{shell} - \delta^{18}O_{water}\right) + 0.12 * \left(\delta^{18}O_{shell} - \delta^{18}O_{water}\right)^2$$

These were then compared with locality-specific instrumental SST data to calculate the offset from expected thermodynamic equilibrium. Monthly SST averages were retrieved from the OSTIA dataset (Good et al., 2020). To compare the calculated isotope derived SST data with the instrumental record, no offset was applied to the water samples. The standard −0.27‰ adjustment (used to align VSMOW scale for water samples with VPDB scale for carbonate samples) was unnecessary, as per the Hays and Grossman (1991) equation (Grossman, 2012).

The coefficient of determination (R^2) was calculated between the oxygen isotope values and the Mg/Ca data (Supplemental Figure S.3–S.16, available online). To calculate this coefficient a linear regression for each unique shell was performed, where $\delta^{18}O$ was modelled as a function of the Mg/Ca ratio. For this analysis, we used the dynamic time-warping method, as suggested by Hausmann et al. (2019a: 8), to align the proxy records. This method is well-suited for comparing time series data with varying lengths and speeds (Netzel and Stepinski, 2017) and was crucial for accurately accounting for differences in growth rates, degrees of time averaging and variations in sampling procedures and resolutions between the $\delta^{18}O$ and Mg/Ca datasets. The dataset and code used for the analysis are available in an OSF repository (Theodoraki et al., 2025) as well as a GitHub repository at https://github.com/Niklas-palaeo/SEAFRONT-ModernReferenceStudy.

Results

LIBS

In total, 400 Mg/Ca maps and 132 Mg/Ca line scans were produced from the shells of the 131 live-collected limpets. Mg/Ca data revealed predictable seasonal cyclicity in almost all specimens (92%, see the example in Figure 3) and in four out of five cases (79%) the actual season of collection was reflected in the Mg/Ca maps. A well-defined seasonal cyclicity means that the

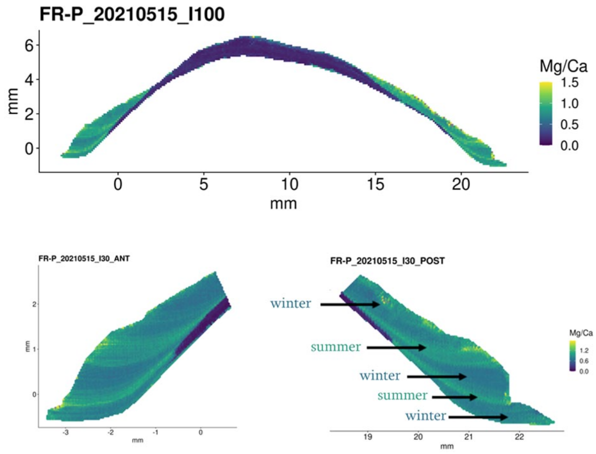

Figure 3. An example from Franchthi with well-defined seasonal cyclicity: Sample FR-P_20210515_I, 100 µm scan of the whole shell section and 30 µm scan of the anterior and the posterior edge. For line scan and isotope data see Figure 5. Two summers were recorded (narrow increments, high Mg/Ca values) and three broader increments (lower Mg/Ca values) reflecting winters.

winter and summer increments are distinctly separated due to their respective intensity ratios (i.e. winter bands around 0.6 and summer bands around 0.8 Mg/Ca intensity ratio). Generally, younger specimens with less than 1 year of growth lack the range in Mg/Ca intensity ratios to make out individual seasons and are thus more ambiguous in their interpretation. When molluscs were more than one-year old, seasonal cyclicity could be more clearly identified and interpreted. However, the Mg/Ca data of young (less than 1 year old) and fast-growing specimens were more challenging to interpret. Young specimens did not exhibit clear seasonal cyclicity patterns so that the seasonal Mg/Ca change could not be properly recognised with LIBS.

The shape of the seasonal growth increments varied among the different localities, but specimens from the same site tended to share similar seasonal growth patterns. The more frequent pattern in the Mg/Ca data observed in this set of samples consisted of extensive winter increments and narrower and more pronounced summers.

Among the 122 specimens with a known season of collection, 80% of the cases were correctly identified based on the Mg/Ca data (see Supplemental Material II, available online). At 10 localities (Agios Petros Kyra Panagia, Plakes Volos, Katiyorgis, Glaros Rethymno, Kedrodasos, Alyko Naxos, Pyrgos Apollonias, Faro Punta Sottile (east) and Faro Punta Sottile (west)), the success rate of the seasonal interpretation (i.e. 'actual') was 100%, while at Koropi, Tonnara del Secco (east) and Youra island (west coast) it was equal to or above 80%. At Nea Kallikrateia and Youra island (south coast) the success rate was close to 75%, while at Franchthi it was 71%. Success rates at Tonnara del Secco (west) and Sousa were 67%, and 50% at both Kokkino in Kyra Panagia and Ligres in Rethymno. At Monemvasia, the season of collection could only be identified in 40% of the cases. The two shell samples from Ysterni Paros, indicated the preceding season of collection (i.e. spring instead of summer). To note, the low success rates only occurred at sites with small sample numbers (Table 2).

Younger specimens (less than 1 year old) did not allow for precise season-of-collection estimates, and usually, these younger specimens were present at highly frequented beaches where human impact and exploitation of the marine environment was more intense. This way, specimens from more touristic and overexploited regions such as Crete or the Cyclades (Kedrodasos, Alyko Naxos, Ligres Rethymno) tended to be younger and gave less accurate results in terms of seasonal variability, while specimens from Agios

Table 2. Successful estimation of the season of collection (%) in comparison with the actual season of collection, grouped by location.

Location name	Number of specimens	Preceding (%)	Preceding/ Actual (%)	Actual (%)	Subsequent (%)	Unknown (%)
Franchthi Paralia	24	13		71	8	8
Monemvasia	5	20		40		40
Youra isl. (west)	12		8	92		
Youra isl. (south)	8	13	13	75		
Agios Petros, Kyra Panagia	15			100		
Kokkino, Kyra Panagia	4	50		50		
Patitiri, Alonnisos	5	20		60		20
Plakes, Volos	3			100		
Koropi	5			80		20
Katiyorgis	6			100		
Ligres, Rethymno	2		50	50		
Glaros, Rethymno	1			100		
Kedrodasos	1			100		
Alyko, Naxos	3			100		
Ysterni, Paros	2	100				
Nea Kallikrateia	4			75		25
Pyrgos Apollonias	2			100		
Tonnara del Secco (east)	5			80		20
Tonnara del Secco (west)	3		33	67		
Faro Punta Sottile (east)	4			100		
Faro Punta Sottile (west)	5			100		
Sousa	3			67		33
Total	122	8	3	80	2	8

The columns represent the relationship between LIBS results and the true season: 'Preceding' indicates LIBS results reflected the preceding season of collection in comparison with the actual one; 'Preceding/Actual' indicates a liminal phase where elemental data allowed interpretation as either preceding or actual; 'Actual' indicates that LIBS results matched the actual season of capture; 'Subsequent' indicates that LIBS results reflected the subsequent season of collection; and 'Unknown' indicates LIBS results showed no interpretable seasonal cyclicity patterns.

Petros and Youra, less frequented uninhabited islands, had the longest-lived specimens among the 22 studied localities. In addition, the island of Youra is part of an ecologically protected marine zone (the National Marine Park of Alonnisos Northern Sporades) where human intervention is nowadays minimal.

Oxygen isotope data

Water and shell aperture samples. Six water samples were collected from coastal areas in Greece and Italy for oxygen isotope analysis (Table 3). Each water sample was measured twice and the results were averaged. The results of the water isotope composition reflected a range of values typical for the Mediterranean region (Dämmer et al., 2020; Gat et al., 1996; Pierre, 1999). Franchthi Paralia had the highest $\delta^{18}O$ value (2.38‰ VSMOW), while the east Tonnara del Secco location had the lowest (0.37‰). Generally, these values are in accordance with the east-west $\delta^{18}O_{water}$ gradient, with values more than 0.45‰ higher in the eastern Mediterranean than the western Mediterranean (Ayache et al., 2024). Tonnara del Secco (east) and Tonnara del Secco (west) had different values though they were collected from nearby sites. Faro Punta Sottile (west) yielded a value of 1.12‰ which was quite close to the value of Tonnara del Secco (west) (1.09‰). The results from Youra island (south coast) and from Agios Petros island that are also from neighbouring islands had similar values (1.27‰ and 1.58‰ respectively).

Samples taken from the aperture, representing the most recent shell growth prior to death, were extracted from twenty specimens collected from different locations at different times of the year (Table 3). These so-called apertural samples showed more inconsistency than would be expected for the shell margin that formed at the same time. The apertural samples ($n=10$) from Franchthi ranged from 1.11‰ to 0.52‰ with an average of 0.78‰ and a median of 0.8‰. Youra island samples ranged from −0.04‰ to 1.32‰ (average = 0.91‰, median = 1.17‰). Faro Punta Sottile had a narrower range of 1.48 to 1.85‰, averaging 1.63‰ (median = 1.55‰), while Tonnara del Secco exhibited values between −0.19 and 1.03‰, with an average of 0.49‰ and a median of 0.64‰. To identify outliers that could disproportionately impact the mean values for each location, we applied a modified z-score method. This approach flags values exceeding 3.5 median absolute deviation (MAD) units from the median (i.e. the highest and lowest values from Franchthi specimens D, E and J, and the much lower value of –0.04‰ at Youra), effectively reducing the influence of outliers (Figure 4, Supplemental Material III, available online).

Calculated SSTs ($T_{\delta^{18}O}$) using the Hays and Grossman equation based on shell aperture ($\delta^{18}O_{shell}$) and water ($\delta^{18}O_{water}$) values were compared with instrumental SSTs at the time of collection of the respective specimens and offsets between measured and estimated SST values determined (Table 3). These offsets (+0.85‰ for Franchthi, –2.35‰ for Youra isl., –1.43‰ for Faro Punta Sottile, and –0.46‰ for Tonnara del Secco) are restricted to the individual sampling months (May for Franchthi, Faro Punta Sottile, and Tonnara del Secco, and September for Youra isl.) and not reflective of the relationship between $\delta^{18}O_{shell}$ and actual SST.

Sequential samples. Fourteen modern shells were sampled sequentially for oxygen isotope analysis, namely, four modern shells from each, Franchthi Paralia (FR-P_20210515_C, G-I) and the small island of Youra in Central Greece (Y-S_20210917_A and C, Y-W_20210917_B and G) and three specimens each from Faro Punta Sottile (FPS-W_20230518_A, FPS-E_20230518_C and D) and Tonnara del Secco (TS-E_20230516_A and B, TS-W_20230516_B) in Sicily (Table 3). All $\delta^{18}O$ curves showed quasi-sinusoidal patterns. More specifically, sequential sampling revealed cyclic changes in isotope values, with minimum and maximum $\delta^{18}O$ values ranging from −0.65‰ to 1.75‰ at Franchthi,

Table 3. $\delta^{18}O_{water}$, instrumental SSTs, $\delta^{18}O_{shell}$ and differences between calculated SSTs ($T_{\delta^{18}O}$) and instrumental SST (after Prendergast and Schöne, 2017: Table 2).

Sample name	Number of $\delta^{18}O$ samples extracted per shell	$\delta^{18}O_{water}$ (‰ VPDB)	Instrumental SST (°C)	$\delta^{18}O$shell aperture (‰ VPDB)	$T_{\delta^{18}O}$(°C) (no offset)	Instrumental SST and $T_{\delta^{18}O}$ (no offset) difference	Applied offset (‰)	$T_{\delta^{18}O}$(°C) (with offset)	Instrumental SST and $T_{\delta^{18}O}$ (with offset) difference
FR-P_20210515_A	1	2.38	19.01	0.80	22.93	−3.92	+0.85	18.99	0.02
FR-P_20210515_B	1	2.38	19.01	0.83	22.78	−3.77	+0.85	18.84	0.17
FR-P_20210515_C	27	2.38	19.01	0.82	22.84	−3.83	+0.85	18.90	0.11
FR-P_20210515_D	1	2.38	19.01	1.11	21.44	−2.43	+0.85	17.56	1.45
FR-P_20210515_E	1	2.38	19.01	0.52	24.25	−5.24	+0.85	20.25	−1.24
FR-P_20210515_F	1	2.38	19.01	0.78	22.99	−3.98	+0.85	19.04	−0.03
FR-P_20210515_G	23	2.38	19.01	0.81	22.85	−3.84	+0.85	18.91	0.10
FR-P_20210515_H	15	2.38	19.01	0.69	23.43	−4.42	+0.85	19.46	−0.45
FR-P_20210515_I	38	2.38	19.01	0.84	22.71	−3.70	+0.85	18.78	0.23
FR-P_20210515_J	1	2.38	19.01	0.64	23.65	−4.64	+0.85	19.68	−0.69
Y-S_20210917_A	29	1.27	26.87	1.19	16.05	10.82	−2.35	27.00	0.13
Y-S_20210917_C	15	1.27	26.87	1.32	15.48	11.39	−2.35	26.35	−0.51
Y-W_20210917_B	17	1.27	26.87	−0.04	21.62	5.25	−2.35	33.27	6.40
Y-W_20210917_G	7	1.27	26.87	1.15	16.23	10.64	−2.35	27.20	0.33
FPS-W_20230518_A	26	1.12	20.66	1.47	14.16	6.50	−1.43	20.52	−0.15
FPS-E_20230518_C	28	1.12	20.66	1.84	12.61	8.05	−1.43	20.04	−0.62
FPS-E_20230518_D	16	1.12	20.66	1.54	13.86	6.80	−1.43	21.40	0.74
TS-E_20230516_A	24	0.37	18.59	0.63	22.93	−4.34	−0.46	16.57	−2.02
TS-E_20230516_B	24	0.37	18.59	−0.18	18.18	0.41	−0.46	20.28	1.69
TS-W_20230516_B	24	1.09	18.59	1.03	15.98	2.61	−0.46	19.69	0.63

SST was calculated from measured $\delta^{18}O_{shell}$ apertural values and $\delta^{18}O_{water}$ using the equation by Hays and Grossman (1991). Calculated SSTs ($T_{\delta^{18}O}$), are shown both with and without the calculated for each location offset applied to $\delta^{18}O_{shell}$.

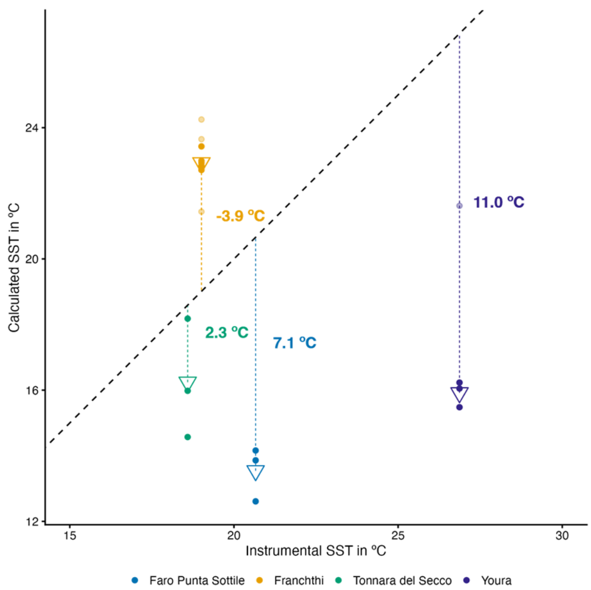

Figure 4. Comparison of calculated SST ($T_{\delta^{18}O}$) (after Hays and Grossman, 1991) with instrumental SST at four sites (Good et al., 2020). SST based on raw $\delta^{18}O_{shell}$ values with no correction. Triangles show mean values by location, excluding outliers identified by a modified z-score (values more than 3.5 MAD units from the median), which reduces the influence of extreme deviations. Text indicates the offset between the mean values and instrumental SST.

−0.04‰ to 2.31‰ at Youra, −0.49‰ to 2.24‰ at Faro Punta Sottile, and −0.97‰ to 1.88‰ at Tonnara del Secco. The seasonal $\delta^{18}O_{shell}$ amplitude at Franchthi (2.40‰) was nearly identical to that at the island of Youra (2.35‰). Studied shells from Faro Punta Sottile revealed a slightly higher amplitude of 2.73‰, whereas at Tonnara del Secco the largest range was 2.85‰.

The coefficient of determination (R^2) was calculated between the oxygen isotope values and the Mg/Ca data (Supplemental Figures S.2–S.15, available online). To calculate this coefficient a simple linear regression for each unique shell was performed, where $\delta^{18}O$ was modelled as a function of the Mg/Ca ratio. For this analysis, we used the dynamic time-warping method, as suggested by Hausmann et al. (2019a: 8), to align the proxy records. This method was crucial for accurately accounting for differences in growth rates, degrees of time averaging and variations in sampling procedures and resolutions between the $\delta^{18}O$ and Mg/Ca datasets. Data measured in all modern live-collected limpets showed a strong linear relationship, as indicated by the high R^2 values. These values ranged from $R^2=0.71$ ($p<0.001$ for shell Y-S_C) to $R^2=0.98$ ($p<0.001$ for shells TS-E_B and TS-W_B), with an average $R^2=0.89$. This relationship is negative, as shown by the corresponding Pearson correlation coefficients (R), which ranged from −0.84 (Y-S_C) to −0.99 (TS-E_B and TS-W_B), with an average of −0.94. $\delta^{18}O_{shell}$ and Mg/Ca values exhibited the strongest mathematical correlation in the samples from Tonnara del Secco (average $R^2=0.98$, $R=-0.99$) and weakest in the samples from Youra (average $R^2=0.84$, $R=-0.92$).

For the four modern samples (FR-P_20210515_C, G, H and I) at Franchthi, the isotope data correlated well with the Mg/Ca data and the known season of capture (spring) was well reflected on both sets of data (Figure 5). As detailed in the Methods section, spring was identified using LIBS by observing increasing Mg/Ca values in the most recent growth increments following winter growth, which were characterised by low Mg/Ca values.

Shell oxygen isotope data of the Faro Punta Sottile group of samples compared well with the Mg/Ca data (Figure 6). The oxygen isotope values at the aperture of all three samples did not differ much from each other (1.48‰, 1.85‰, 1.55‰). All three samples reflected the known season of collection (spring).

Results from Tonnara del Secco compared well with the Mg/Ca line scans. From the three samples, samples TS-E_20230516_B and TS-W_20230516_B reflected the expected rising spring temperatures (Figure 7). The latter did not yield significantly low winter $\delta^{18}O$ values in its winter increments compared to the other

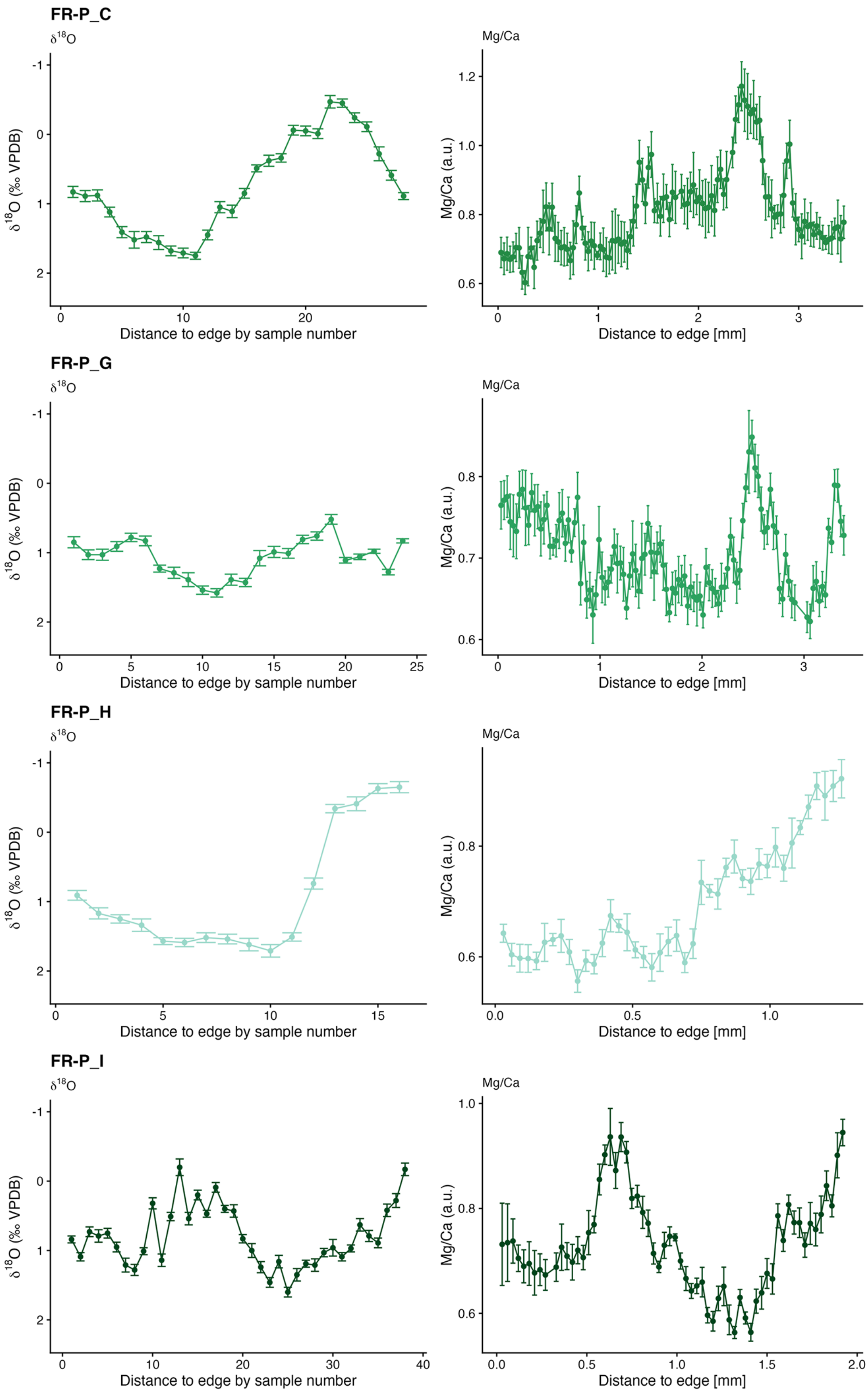

Figure 5. Sequential samples. Oxygen isotope profiles of samples FR-P_20210515_C and G to I compared to Mg/Ca ratio line scans. Error bars represent analytical uncertainty ($\pm 1\sigma$) for each measurement.

two samples from the same location by recording a smaller range of annual temperature variation Apertural values of specimen TS-E_20230516_A were relatively low indicating winter season of collection.

Isotope results from the samples from Youra (Figure 8) are less well-defined when compared to their respective Mg/Ca data. This is due to the very restricted calcitic area of these shells where the sampling took place. Seasonally resolved increments were compacted together in an area of a few millimetres as the shell growth was condensed. In this case micromilling did not provide the necessary sampling resolution required to properly resolve the seasonal change in $\delta^{18}O_{shell}$. Time-averaging is evident in these samples, especially in samples Y-S_20210917_C and Y-W_20210917_G, where the sampled surface of the latter had a length of only 1.5 mm. Isotope results of samples Y-W_20210917_B and Y-S_20210917_A, compared better with the Mg/Ca data demonstrating seasonal cyclicity patterns.

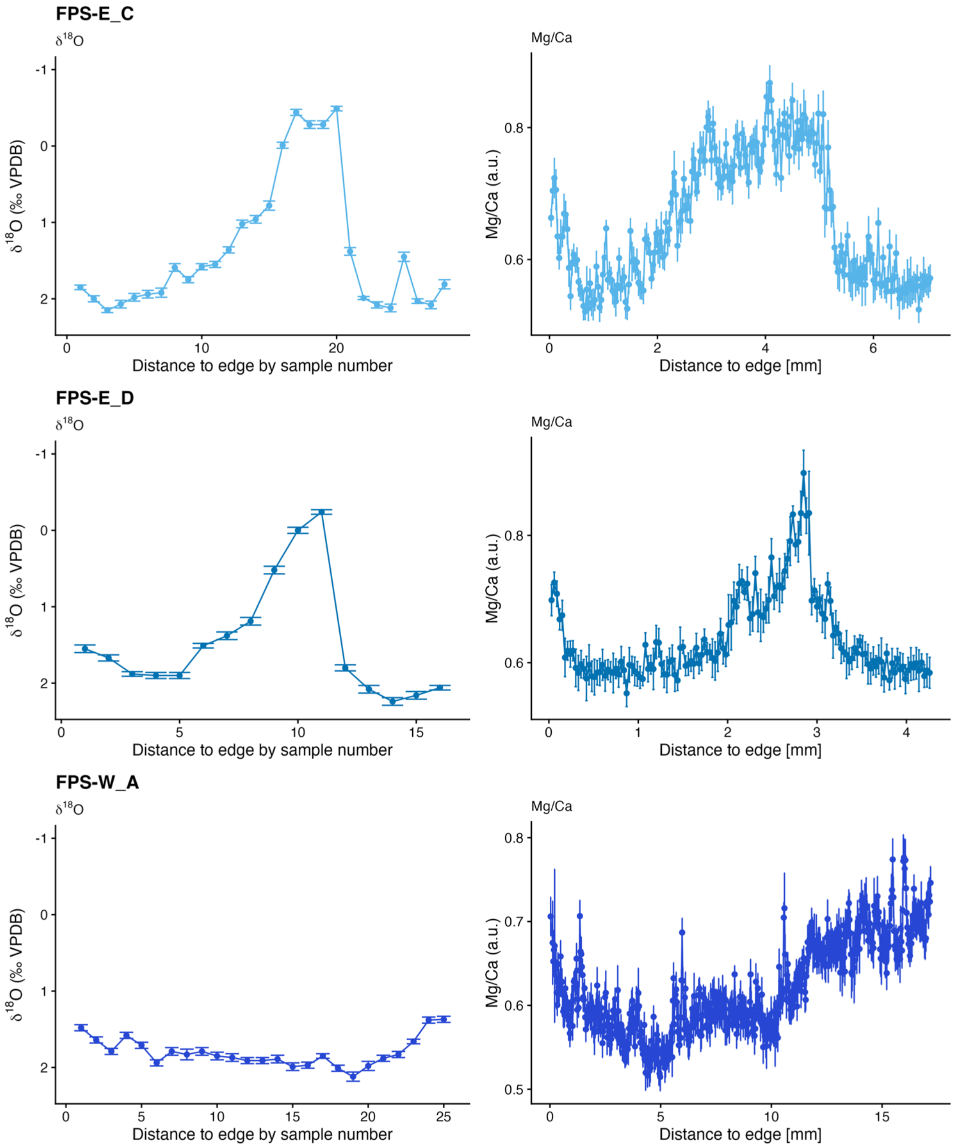

Figure 6. Sequential samples. Oxygen isotope profiles of samples from Faro Punta Sottile in Sicily compared to Mg/Ca ratio line scans. Error bars represent analytical uncertainty (±1σ) for each measurement.

Discussion

Correlation of Mg/Ca and $\delta^{18}O_{shell}$

This study represents a comparative analysis of Mg/Ca ratios in modern *P. caerulea* specimens, focusing on both Mg/Ca ratios and $\delta^{18}O$ values as palaeotemperature proxies. Here, we found a strong correlation between both chemical properties with R^2 values ranging from 0.71 to 0.98 (average $R^2=0.89$, $R=-0.94$) (Figure 9).

In shells from Tonnara del Secco the correlation between $\delta^{18}O_{shell}$ and Mg/Ca_{shell} was the strongest (average $R^2=0.98$, $R=-0.99$), followed by Faro Punta Sottile (average $R^2=0.91$, $R=-0.95$). These figures further substantiate the use of limpets as reliable archives for palaeotemperature reconstructions, aligning with and extending previous research on *Patella* spp. and related species across different geographic regions. Ferguson et al. (2011) found a good correlation $R^2=0.79$, while Hausmann et al. (2019a) observed values exceeding $R^2>0.80$ for *P. caerulea*. García-Escárzaga et al. (2021) found R^2 values for *P. depressa* that range from 0.78 to 0.87 and Hausmann et al. (2024) an $R^2=0.89$ for *P. vulgata*. Other limpet species such as *Nacella* produced high correlations ($R^2=0.95$) (Hausmann et al., 2024).

Ideally, the correlations and regression curves should be more consistent across locations and species, but factors additionally influencing the Mg/Ca ratios beyond SST have not yet been fully captured: Firstly, different sampling resolutions employed in each study would lead to variable detection of extreme values and thus differences in total range, particularly in combination with differences in ontogenetic age and variable growth rate. Ontogenetic age may affect the amount of Mg substituting for Ca in the crystal lattice of calcite and variable growth rate can affect the time represented by each data point (e.g. visible in specimen Y-W_G with smaller range of values than other, coeval specimens from the island of Youra). Secondly, discrepancies in equipment sensitivity and measurement accuracy across the different studies (e.g. LIBS and ICP-OES (García-Escárzaga et al., 2018)) could influence the consistency of correlations. Lastly, and most importantly, different positions of line scans along the growth increment itself can also influence the measured Mg/Ca ratio, because the Mg/Ca ratio is not consistent within one increment (Hausmann et al., 2019a; Lazareth et al., 2013; Mirapeix et al., 2025). Thus, different line scans of the same shell can produce different Mg/Ca ratios and regression curves with different slopes. Mirapeix et al. (2025) apply virtual sampling of 2D maps to take the overall range of Mg/Ca ratios within one increment into account rather than picking one specific line, but given that this intra-increment variability of Mg/Ca ratios varies in intensity from one specimen to

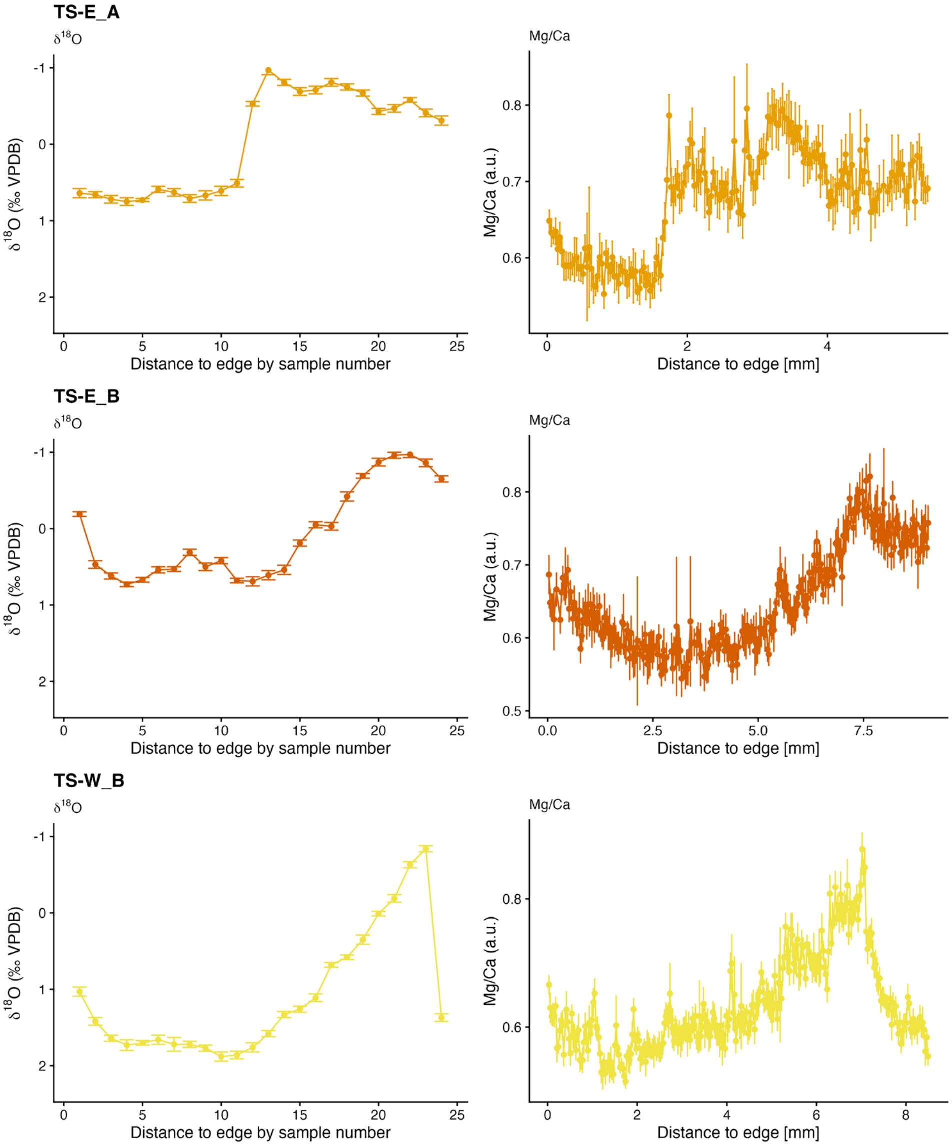

Figure 7. Sequential samples. Oxygen isotope profiles of samples from the Tonnara del Secco location in Sicily (TS-E_20230516_A and B, TS-W_20230516_B) compared to Mg/Ca ratio line scans. Error bars represent analytical uncertainty ($\pm 1\sigma$) for each measurement.

another, virtual sampling would not produce identical regression curves for different specimens.

The present study is the largest collection of modern limpet shells used to determine the relationship between both temperature proxies and provides some statistical insight into how reliable *P. caerulea* is for larger regions. This large number of specimens was achieved by using rapid Mg/Ca analyses, which allowed the identification of the rate of the shell growth as well as the required sampling resolution for oxygen isotope analysis and thus minimising the amount of oxygen isotope samples required per specimen. This approach bridges the gap between sample sizes and resolutions, addressing the traditionally high cost and time demands of sclerochronological analysis, which typically limits high-resolution sampling (West et al., 2018).

SST reconstruction using $\delta^{18}O_{shell}$

Previous studies from other areas suggest a range of offsets (from +0.36‰ to +1.01‰) to correct the $\delta^{18}O_{shell}$ values from *Patella* shells and to calibrate the archaeological shell results for palaeotemperature equations (Fenger et al., 2007; Ferguson et al., 2011; Gutiérrez-Zugasti et al., 2017; Shackleton, 1973). For the Central and Eastern Mediterranean region, an offset of –0.72‰ was previously reported based on 24 shells from a single location in Sousa, Libya and then applied to the Central Mediterranean (Prendergast and Schöne, 2017). Despite the overlapping research area, this offset was not applicable to the samples of the present study as they produced largely deviating values from the instrumental data

Here, we calculated the SST values ($T_{\delta^{18}O}$) for each location using the apertural $\delta^{18}O$ values and $\delta^{18}O_{water}$ values, and compared them with the instrumental SST values. These $T_{\delta^{18}O}$(°C) values were deviating from the instrumental values with differences ranging from −5.24°C to −2.43°C for Franchthi, 5.25°C to 11.39°C for Youra, 6.50°C to 8.05°C for Faro Punta Sottile and −4.34°C to 2.61°C for Tonnara del Secco (see Table 3).

What precisely controls these offsets remains elusive until further studies with higher resolved environmental data and more frequent shell and water sample collection throughout the year have taken place. While the sample locations do not experience any short-term freshwater inflow from for example, rivers we cannot rule out hourly, daily or weekly fluctuations of the $\delta^{18}O_{water}$ due to for example, evaporation. These fluctuations could explain the intra-site variability as well as the locality-specific offsets, with more water samples to capture the short-term $\delta^{18}O_{water}$ variability being the next step. Prendergast and Schöne (2017)

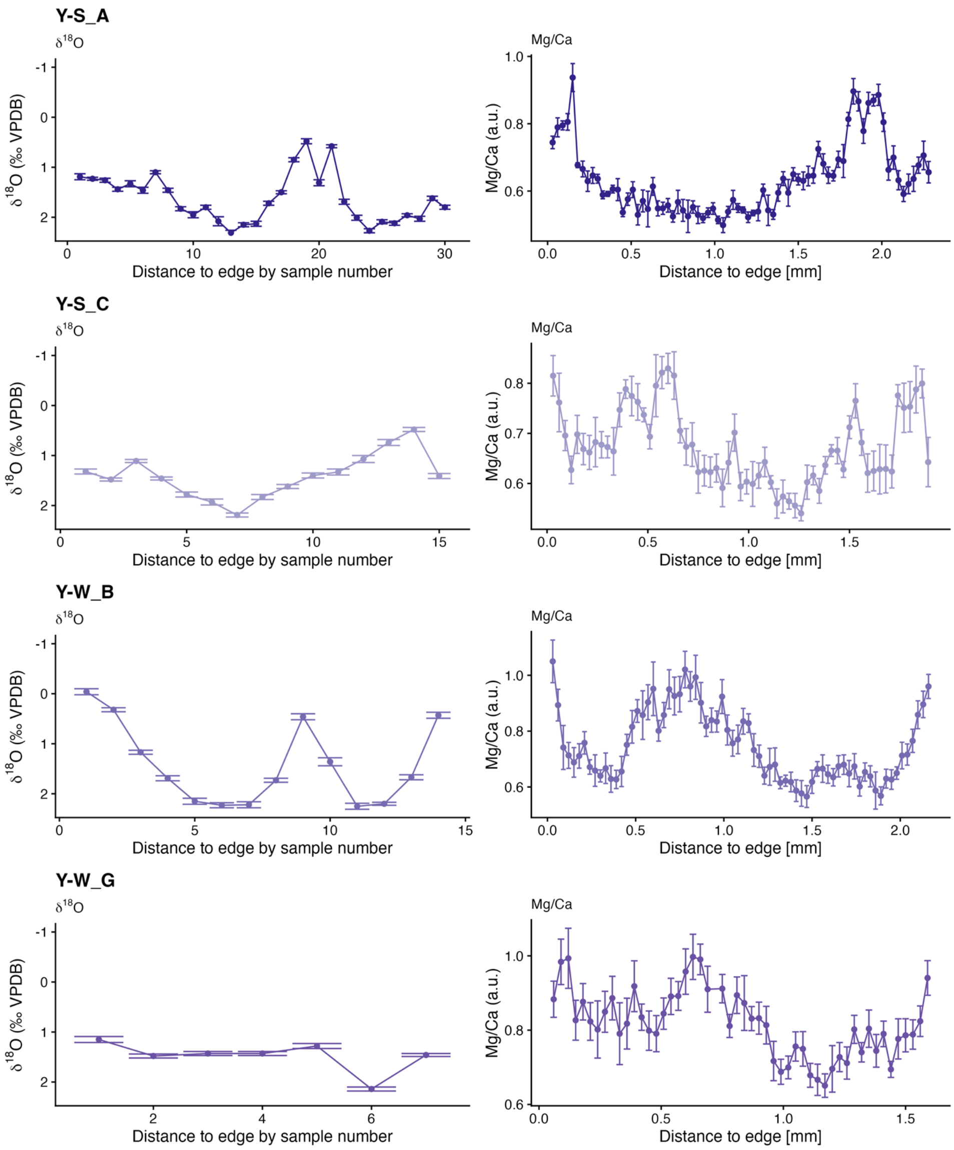

Figure 8. Sequential samples. Oxygen isotope profiles of samples from Youra compared to Mg/Ca ratio line scans. Error bars represent analytical uncertainty (±1σ) for each measurement.

suggest differences in growth rates during certain seasons that might also affect individual animals differently. Lab-based studies have not been carried out to rule out microenvironmental influences, but are likely the way forward.

Conclusion

This study represents the largest comparative analysis of Mg/Ca ratios in modern mollusc shells to date. Focusing on both Mg/Ca ratios and $\delta^{18}O$ values as proxies for reconstructing seasonality patterns and palaeotemperature it offers a robust dataset for the use of limpets as palaeotemperature proxies. Our study found a high average correlation ($R^2=0.89$) between Mg/Ca ratios and SST in *P. caerulea* specimens, underscoring Mg/Ca as a reliable proxy for relative SST changes. The $\delta^{18}O$ analysis of shells and water samples at selected localities reliably estimated SST values for the seasons of sample collection (May, September), after applying empirical offsets that helped align with instrumental SST data. These offsets, however, vary seasonally and across regions, emphasising the need for site-specific adjustments when applying palaeotemperature equations in archaeological contexts. Our Mg/Ca data exhibited well-defined seasonal cyclicity, with 79% of specimens reflecting the known season of collection. However, seasonal interpretations were less reliable in younger, fast-growing molluscs, suggesting that age and growth rate affect the clarity of seasonal patterns and are problems that might require even higher resolved analyses. Additionally, this study provides a robust baseline for using *P. caerulea* as a palaeoclimate proxy, particularly in the Mediterranean. The calibration dataset supports broader applications, with location-specific calibrations enhancing its potential for palaeoclimate reconstructions at archaeological sites.

The research highlights the advantage of Mg/Ca mapping as a preliminary diagnostic technique prior to conducting oxygen isotope analysis, improving the accuracy and reliability of temperature reconstructions. The combination of Mg/Ca and $\delta^{18}O$ data in *P. caerulea* offers a reliable and fast method for reconstructing past SST and seasonal patterns, after applying site-specific adjustments. This dataset will aid future palaeoclimate studies, advancing our understanding of historical climate dynamics in the Mediterranean region. In particular, Mg/Ca mapping facilitates the detection of seasonal cyclicity, such as the alternation between winter and summer conditions. By identifying these clear seasonal patterns, researchers can analyse and evaluate the

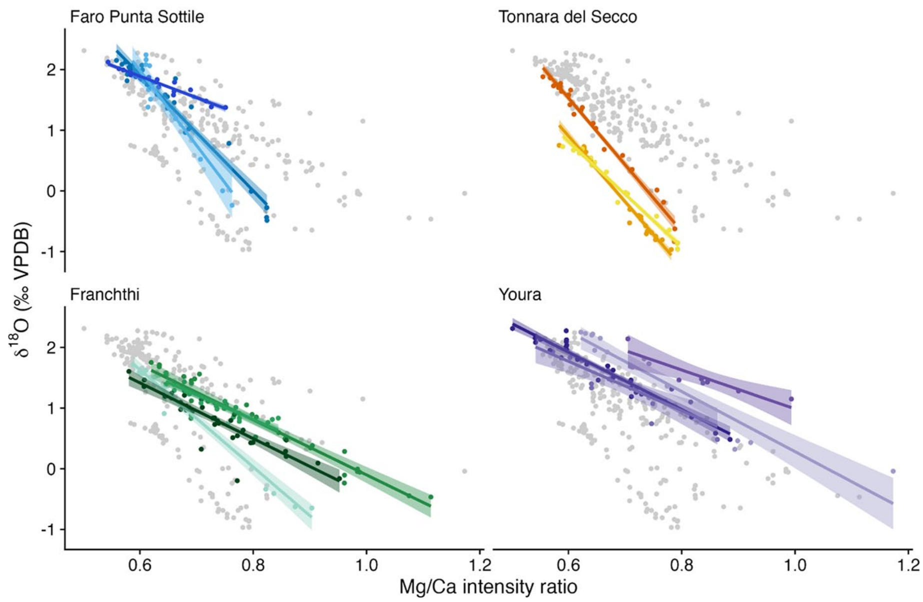

Correlation Table

Shell	R2 value	p-value
Faro Punta Sottile		
FPS-E_C	0.95	1e-18
FPS-E_D	0.84	7e-07
FPS-W_A	0.94	3e-15
Franchthi		
FR-P_C	0.91	2e-15
FR-P_G	0.84	3e-10
FR-P_H	0.96	2e-11
FR-P_I	0.78	1e-13
Tonnara del Secco		
TS-E_A	0.97	9e-19
TS-E_B	0.98	4e-20
TS-W_B	0.98	7e-20
Youra		
Y-S_A	0.93	3e-17
Y-S_C	0.71	8e-05
Y-W_B	0.89	1e-08
Y-W_G	0.82	5e-03

Figure 9. Collated correlation graphs grouped by region comparing the Mg/Ca data and oxygen isotope data of all *14* modern specimens that were sampled sequentially. Colours are assigned by shell specimen and location with grey points in the background showing all other locations' data points as a reference.

molluscan record before conducting isotope analysis, while also detecting potential physiological traits that may interfere with interpreting the elemental record (Hausmann et al., 2019a).

Acknowledgements

This article was made possible with funding from the DFG under the Emmy Noether Program (project number: 439799406). The authors thank the Applied Photonics Lab of the Institute of Electronic Structure and Laser of the Foundation for Research and Technology – Hellas for close support with the LIBS system. We further thank Dr. Hubert Vonhof for the analysis of water samples at the Max Planck Institute for Chemistry in Mainz as well as for comments and suggestions on an earlier version of the manuscript.

A survey permit was acquired by the Greek Ministry of the Environment and Energy to collect specimens from the National Marine Park of Alonissos-Northern Sporades for granting the survey permit necessary for collecting modern shell specimens on the islands of Kyra Panagia and Youra (protocol number: ΥΠΕΝ/Δ ΔΔ/29195/996). We thank Stefanos Paraskevopoulos, Spyros Iossifidis and Angeliki Kita for assisting us with our work in the area. Modern samples were also provided by Tatiana Andreovits, Manos Papageorgiou and Panagiotis Keramidas. Lastly, we thank Igor Gutiérrez-Zugasti for helpful comments and suggestions for the final manuscript.

Author contributions

Danai Theodoraki: Conceptualisation; Data curation; Formal analysis; Investigation; Methodology; Validation; Visualisation; Writing – original draft; Writing – review & editing.
Marcello Mannino: Resources; Validation; Writing – review & editing.
Amy Prendergast: Resources.
Bernd Schöne: Resources; Validation; Writing – review & editing.
Niklas Hausmann: Conceptualisation; Data curation; Formal analysis; Funding acquisition; Investigation; Methodology; Project administration; Resources; Software; Supervision; Validation; Visualisation; Writing – original draft; Writing – review & editing.

Data availability

All data generated or analysed during this study are included in this published article and its supplementary information files. All underlying data files are available in an OSF repository (Theodoraki et al., 2025) as well as a GitHub repository at https://github.com/Niklas-palaeo/SEAFRONT-ModernReferenceStudy. Any additional data not included in the manuscript can be provided by the corresponding author upon reasonable request. We believe in the importance of open science and are committed to sharing our data to encourage further research and collaboration.

Funding

The authors disclosed receipt of the following financial support for the research, authorship, and/or publication of this article: This work was supported by the Deutsche Forschungsgemeinschaft (DFG) under the Emmy Noether Program (project number: 439799406).

ORCID iDs

Danai Theodoraki https://orcid.org/0009-0006-2095-177X
Amy L Prendergast https://orcid.org/0000-0002-4970-9956
Bernd R Schöne https://orcid.org/0000-0002-6879-1633
Niklas Hausmann https://orcid.org/0000-0002-4381-8334

Supplemental material

Supplemental material for this article is available online.

References

Ayache M, Dutay JC, Mouchet A et al. (2024) Modelling the water isotope distribution in the Mediterranean Sea using a high-resolution oceanic model (NEMO-MED12- watiso v1. 0): Evaluation of model results against in situ observations. *Geoscientific Model Development* 17(17): 6627–6655.

Aydogdu A, Miraglio P, Escudier R et al. (2023) The dynamical role of upper layer salinity in the Mediterranean Sea. *State of the Planet* 1: 1–9.

Bar-Yosef Mayer DE (2005) An introduction to archaeomalacology. In: Bar-Yosef Mayer DE (ed.) *Archaeomalacology:*

Molluscs in Former Environments of Human Behaviour. Oxford: Oxbow Books, pp.1–4.

Çakirlar C (2014) Molluscs (invertebrates): Analyses in environmental Archaeology. In: Smith C (ed.) *Encyclopedia of Global Archaeology*. New York, NY: Springer, pp.5005–5010.

Claassen C (1998) *Cambridge Manuals in Archaeology: Shells*. Cambridge: Cambridge University Press.

Cobo A, García-Escárzaga A, Gutiérrez-Zugasti I et al. (2017) Automated measurement of magnesium/calcium ratios in gastropod shells using laser-induced breakdown spectroscopy for paleoclimatic applications. *Applied spectroscopy* 71(4): 591–599.

Colonese AC, Camarós E, Verdún E et al. (2011) Integrated archaeozoological research of shell middens: New insights into hunter-gatherer-fisher coastal exploitation in Tierra Del Fuego. 6(2): 235–254.

Colonese AC, Verdún-Castelló E, Álvarez M et al. (2012) Oxygen isotopic composition of limpet shells from the Beagle Channel: Implications for seasonal studies in shell middens of Tierra del Fuego. *Journal of Archaeological Science* 39(6): 1738–1748.

Craig H (1957) Isotopic standards for carbon and oxygen and correction factors for mass-spectrometric analysis of carbon dioxide. *Geochimica et cosmochimica acta* 12(1-2): 133–149.

Cremers D and Radziemski L (2006) *History and Fundamentals of Libs. Laser Induced Breakdown Spectroscopy: Fundamentals and Applications*. Cambridge: Cambridge University Press, pp.9–16.

Cremers DA and Radziemski LJ (2013) *Handbook of Laser-Induced Breakdown Spectroscopy*. Nashville, TN: John Wiley & Sons.

Dämmer LK, de Nooijer L, van Sebille E et al. (2020) Evaluation of oxygen isotopes and trace elements in planktonic foraminifera from the Mediterranean Sea as recorders of seawater oxygen isotopes and salinity. *Climate of the Past* 16(6): 2401–2414.

de Graaf S, Vonhof HB, Levy EJ et al. (2021) Isotope ratio infrared spectroscopy analysis of water samples without memory effects. *Rapid Communications in Mass Spectrometry* 35(8): e9055.

Deith MR and Shackleton NJ (1988) *Oxygen Isotope Analyses of Marine Molluscs From Franchthi Cave. Marine Molluscan Remains From Franchthi Cave*. Bloomington and Indianapolis, IN: Indiana University Press, pp.133–156.

Epstein S, Buchsbaum R, Lowenstam H et al. (1951) Carbonate-water isotopic temperature scale. *GSA Bulletin* 62(4): 417–426.

Epstein S, Buchsbaum R, Lowenstam HA et al. (1953) Revised carbonate-water isotopic temperature scale. *GSA Bulletin* 64(11): 1315–1326.

European Union-Copernicus Marine Service (2016) Global ocean 1/12° physics analysis and forecast updated daily. Mercator Ocean International. DOI:10.48670/MOI-00016.

Fenger T, Surge D, Schöne B et al. (2007) Sclerochronology and geochemical variation in limpet shells (*Patella vulgata*): A new archive to reconstruct coastal sea surface temperature. *Geochemistry Geophysics Geosystems* 8(7): 1–17.

Ferguson JE, Henderson GM, Fa DA et al. (2011) Increased seasonality in the Western Mediterranean during the last glacial from limpet shell geochemistry. *Earth and Planetary Science Letters* 308(3–4): 325–333.

Firth LB (2021) What have limpets ever done for us? On the past and present provisioning and cultural services of limpets. *International Review of Environmental History* 7(2): 5–45.

García-Escárzaga A, Clarke LJ, Gutiérrez-Zugasti I et al. (2018) Mg/Ca profiles within archaeological mollusc (*Patella vulgata*) shells: Laser-induced breakdown spectroscopy compared to inductively coupled plasma-optical emission spectrometry. *Spectrochimica Acta Part B Atomic Spectroscopy* 148: 8–15.

García-Escárzaga A, Gutiérrez-Zugasti I, González-Morales MR et al. (2020) Shell sclerochronology and stable oxygen isotope ratios from the limpet *Patella depressa* Pennant, 1777: Implications for palaeoclimate reconstruction and archaeology in northern Spain. *Palaeogeography Palaeoclimatology Palaeoecology* 560: 110023.

García-Escárzaga A, Martínez-Minchero M, Cobo A et al. (2021) Using Mg/Ca ratios from the limpet *Patella depressa* Pennant, 1777 measured by laser-induced breakdown spectroscopy (LIBS) to reconstruct paleoclimate. *Applied Sciences* 11(7): 2959.

Gat JR, Shemesh A, Tziperman E et al. (1996) The stable isotope composition of waters of the eastern Mediterranean Sea. *Journal of Geophysical Research Oceans* 101(C3): 6441–6451.

Good S, Fiedler E, Mao C et al. (2020) The current configuration of the OSTIA system for operational production of foundation sea surface temperature and ice concentration analyses. *Remote Sensing* 12(4): 720.

Grossman EL (2012) Applying oxygen isotope paleothermometry in deep time. *The Paleontological Society papers* 18: 39–68.

Gutiérrez-Zugasti I, Suárez-Revilla R, Clarke LJ et al. (2017) Shell oxygen isotope values and sclerochronology of the limpet *Patella vulgata* Linnaeus 1758 from northern Iberia: Implications for the reconstruction of past seawater temperatures. *Palaeogeography Palaeoclimatology Palaeoecology* 475(1): 162–175.

Gutiérrez-Zugasti I, Suárez-Revilla R, García-Escárzaga A, et al. (2025) Shell sclerochronology of the limpet *Patella ferruginea* Gmelin, 1791: Implications for growth patterns and reconstruction of past sea surface temperatures. *Palaeogeography, Palaeoclimatology, Palaeoecology* 670: 112954.

Hallmann N, Burchell M, Schöne BR, et al. (2009) High-resolution sclerochronological analysis of the bivalve mollusk Saxidomus gigantea from Alaska and British Columbia: Techniques for revealing environmental archives and archaeological seasonality. *Journal of Archaeological Science* 36: 2353–2364.

Hausmann N (2024) A current assessment and commentary on the field of shell seasonality. *Archaeological and Anthropological Sciences* 16(9): 153–154. DOI: 10.1007/s12520-024-02056-8

Hausmann N, Prendergast AL, Lemonis A et al. (2019a) Extensive elemental mapping unlocks Mg/Ca ratios as climate proxy in seasonal records of Mediterranean limpets. *Scientific Reports* 9(1): 3698.

Hausmann N, Robson HK and Hunt C (2019b) Annual growth patterns and interspecimen variability in Mg/Ca records of archaeological Ostrea edulis (European Oyster) from the Late Mesolithic site of Conors Island. *Open Quaternary* 5(9): 1–18.

Hausmann N, Siozos P, Lemonis A et al. (2017) Elemental mapping of Mg/Ca intensity ratios in marine mollusc shells using laser-induced breakdown spectroscopy. *Journal of Analytical Atomic Spectrometry* 32(8): 1467–1472.

Hausmann N, Surge D and BrIz I Godino I (2024) Confirmation of Mg/Ca ratios as palaeothermometers in Atlantic limpet shells. *Palaeogeography Palaeoclimatology Palaeoecology* 655: 112538.

Hausmann N, Theodoraki D, Piñon V et al. (2023) Applying laser induced breakdown spectroscopy (LIBS) and elemental imaging on marine shells for archaeological and environmental research. *Scientific Reports* 13(1): 19812.

Hays PD and Grossman EL (1991) Oxygen isotopes in meteoric calcite cements as indicators of continental paleoclimate. *Geology* 19(5): 441–444.

Jacobsen TW, Farrand WR and Cooper FA (1988) *Franchthi Cave and Paralia: Excavations at Franchthi Cave, Greece Fascicle 1: Maps, Plans, and Sections*. Bloomington, MN: Indiana University Press.

King F, Prendergast AL, Frost E et al. (2025) A key to seasonal shellfish exploitation: Elemental mapping of Mg/Ca ratios in Lutruwita (Tasmania) Cellana limpets. *Palaeogeography Palaeoclimatology Palaeoecology* 674: 113023.

Lazareth CE, Le Cornec F, Candaudap F et al. (2013) Trace element heterogeneity along isochronous growth layers in bivalve shell: Consequences for environmental reconstruction. *Palaeogeography Palaeoclimatology Palaeoecology* 373: 39–49.

Leng MJ and Lewis JP (2016) Oxygen isotopes in molluscan shell: Applications in environmental archaeology. *Environmental Archaeology* 21(3): 295–306.

Mannino MA, Thomas KD, Leng MJ et al. (2008) Shell growth and oxygen isotopes in the topshell Osilinus turbinatus: Resolving past inshore sea surface temperatures. *Geo-Marine Letters* 28(5-6): 309–325.

Martínez-Minchero M, Cobo A, Méndez-Vicente A et al. (2023) Comparison of Mg/Ca concentration series from *Patella depressa* limpet shells using CF-LIBS and LA-ICP-MS. *Talanta* 251: 123757.

Mirapeix J, Arniz-Mateos R, García-Escárzaga A et al. (2025) Virtual sampling: Archaeological implications of a new technique for elemental mapping of Mg/Ca ratios in marine mollusc shells. *Journal of Archaeological Science* 173: 106123.

Netzel P and Stepinski TF (2017) World climate search and classification using a dynamic time warping similarity function. In: Griffith D, Chun Y and Dean D (eds) *Advances in Geocomputation*. Cham: Springer International Publishing, pp.181–195.

Ozer T, Gertman I, Gildor H et al. (2022) Thermohaline temporal variability of the SE Mediterranean coastal waters (Israel) – Long-term trends, seasonality, and connectivity. *Frontiers in Marine Science* 8: 1–14.

Parker W, Yanes Y, Mesa Hernández E et al. (2020) Shellfish exploitation in the western canary islands over the last two Millennia. *Environmental Archaeology* 25(1): 14–36.

Pierre C (1999) The oxygen and carbon isotope distribution in the Mediterranean water masses. *Marine Geology* 153(1-4): 41–55.

Poulos SE, Drakopoulos PG and Collins MB (1997) Seasonal variability in sea surface oceanographic conditions in the Aegean Sea (Eastern Mediterranean): An overview. *Journal of Marine Systems* 13(1-4): 225–244.

Prendergast AL and Schöne BR (2017) Oxygen isotopes from limpet shells: Implications for palaeothermometry and seasonal shellfish foraging studies in the Mediterranean. *Palaeogeography Palaeoclimatology Palaeoecology* 484: 33–47.

Schöne BR, Zhang Z, Radermacher P et al. (2011) Sr/Ca and Mg/Ca ratios of ontogenetically old, long-lived bivalve shells (*Arctica islandica*) and their function as paleotemperature proxies. *Palaeogeography Palaeoclimatology Palaeoecology* 302(1-2): 52–64.

Shackleton NJ (1973) Oxygen isotope analysis as a means of determining season of occupation of prehistoric midden sites. *Archaeometry* 15(1): 133–141.

Skliris N, Sofianos SS, Gkanasos A et al. (2011) Long-term sea surface temperature variability in the Aegean Sea. *Advances in Oceanography and Limnology* 2(2): 125–139.

Surge D and Barrett JH (2012) Marine climatic seasonality during medieval times (10th to 12th centuries) based on isotopic records in Viking Age shells from Orkney, Scotland. *Palaeogeography Palaeoclimatology Palaeoecology* 350–352: 236–246.

Theodoraki D, Mannino M, Prendergast A et al. (2025) Data and code multi-regional calibration of *Patella caerulea* as palaeothermometer using oxygen isotope values and Mg/Ca ratios. OSF. Available at: osf.io/6pw3b.

Uçkaç Ş (2005) Sea surface variability in the Aegean Sea. *Ege Journal of Fisheries and Aquatic Sciences* 22(1): 129–135.

Urey HC (1947) The thermodynamic properties of isotopic substances. *Journal of the Chemical Society* 562–581. DOI: 10.1039/jr9470000562

Urey HC, Lowenstam HA, Epstein S et al. (1951) Measurement of paleotemperatures and temperatures of the Upper Cretaceous of England, Denmark, and the southeastern United States. *GSA Bulletin. GeoScienceWorld* 62(4): 399–416.

Wang T, Surge D and Mithen S (2012) Seasonal temperature variability of the neoglacial (3300–2500BP) and Roman warm period (2500–1600BP) reconstructed from oxygen isotope ratios of limpet shells (*Patella vulgata*), Northwest Scotland. *Palaeogeography Palaeoclimatology Palaeoecology* 317-318: 104–113.

West CF, Burchell M and Andrus CFT (2018) Molluscs and paleoenvironmental reconstruction in island and coastal settings: Variability, seasonality, and sampling. In: Giovas CM and LeFebvre MJ (eds) *Zooarchaeology in Practice: Case Studies in Methodology and Interpretation in Archaeofaunal Analysis*. New York, NY: Springer, pp.191–208.